ACS APPLIED MATERIALS & INTERFACES

Research Article

www.acsami.org

Nanospace-Confinement Copolymerization Strategy for Encapsulating Polymeric Sulfur into Porous Carbon for Lithium–Sulfur Batteries

Bing Ding, Zhi Chang, Guiyin Xu, Ping Nie, Jie Wang, Jin Pan, Hui Dou, and Xiaogang Zhang*

Jiangsu Key Laboratory of Materials and Technology for Energy Conversion, College of Material Science and Engineering, Nanjing University of Aeronautics and Astronautics, Nanjing, 210016, P. R. China

Supporting Information

ABSTRACT: Given their high theoretical energy density, lithium–sulfur (Li–S) batteries have recently attracted ever-increasing research interest. However, the dissolution of polysulfides and uncontrolled deposition of insoluble discharge product significantly hinder the cycling stability. Herein, a nanospace-confinement copolymerization strategy for encapsulating polymeric sulfur into porous carbon matrix is presented. The morphologies and sulfur contents of carbon/polymeric sulfur (C/PS) composites could be readily tailored by controlling the copolymerization time. Confining polymeric sulfur in the porous carbon with abundant interparticle pores facilitates rapid electronic/ionic transport and mitigates dissolution of polysulfides intermediates. More importantly, the organic sulfur units dispersed in the insoluble/insulating Li_2S_2/Li_2S phase could prevent its irreversible deposition. Such nanostructure with tailored chemistry property permits the C/PS electrodes to exhibit enhanced cycling stability and high rate capability. The nanospace-confinement copolymerization strategy features general and facial advantages, which may provide new opportunities for the future development of advanced sulfur cathodes.

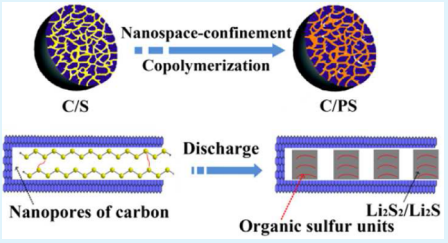

KEYWORDS: *lithium–sulfur batteries, copolymerization, nanospace-confinement, carbon/polymeric sulfur composites, electrochemistry*

INTRODUCTION

Driven by the ever-increasing demand of energy storage in portable electronics, vehicle electrification and smart grid, high-energy rechargeable batteries recently are under intense investigations.[1] Among various types of rechargeable batteries, lithium–sulfur (Li–S) batteries attract extensive attention because of their high theoretical energy density (2600 Wh kg^{-1}) and competitive cost. Li–S batteries typically use elemental sulfur as the cathode and metal lithium as the anode and work through multielectron-transfer reaction of $S_8 + 16Li^+ + 16e^- \leftrightarrow 8Li_2S$.[2,3] During the charge/discharge process, the high dissolution of polysulfides intermediates in the organic electrolyte leads to the shuttle effect and irreversible deposition of Li_2S_2/Li_2S, which are considered as the main reasons for the rapid capacity fading of sulfur cathode.[4−8] In addition, the volume change and ionic/electronic insulation of sulfur and discharged products also hampered the electrochemical performances of sulfur cathode.[9−12]

To tackle the dissolution issue, a promising technology is encapsulating sulfur into a porous and conductive host, such as carbon materials,[13−16] conductive polymers,[17,18] and core–shell or yolk–shell nanostructured materials.[10,11,17,19,20] The pioneered work by Nazar et al. described trapping sulfur species by ordered mesoporous carbon CMK-3.[13] This highly ordered nanostructured cathode exhibited a capacity of about 1000 mAh g^{-1} for 20 cycles. Inspired by this technology, superior nanostructured materials with optimized porous size distribution and tailored surface chemistry have been developed for better trapping sulfur species in the past few years.[21−25] For example, well-defined microporous carbon was employed to prepare small sulfur molecules of S_{2-4}, which could avoid unfavorable transition reaction between S_8 and S_4^{2-}.[21] Carbon materials with reactive functional groups[26] or nitrogen-doping[27,28] were reported to trap the polysulfides more effectively through chemical interactions. Despite the successful demonstrations based on these diverse materials with different nanostructures, however, there are still some polysulfides leaching out.[29,30] This is mainly because the encapsulation technology just slows down the dissolution of polysulfides but does not totally eliminate this phenomenon. Moreover, the electromigration of polysulfides is hard to overcome by the encapsulation technology merely. The dissolution of polysulfides not only leads to the losing of active materials but also is directly associated with the irreversible deposition of insoluble/insulating Li_2S_2/Li_2S on the surface of cathode.[31−33] The accumulation of detrimental Li_2S_2/Li_2S deposition could block the electronic/ionic transport, which is another important reason for rapid capacity fading. Manthiram and Xiao et al.[34,35] described that charge operation control could quantitatively control the thickness and uniformity of Li_2S_2/Li_2S redeposited

Received: January 29, 2015
Accepted: May 13, 2015
Published: May 13, 2015

DOI: 10.1021/acsami.5b00870
ACS Appl. Mater. Interfaces 2015, 7, 11165−11171

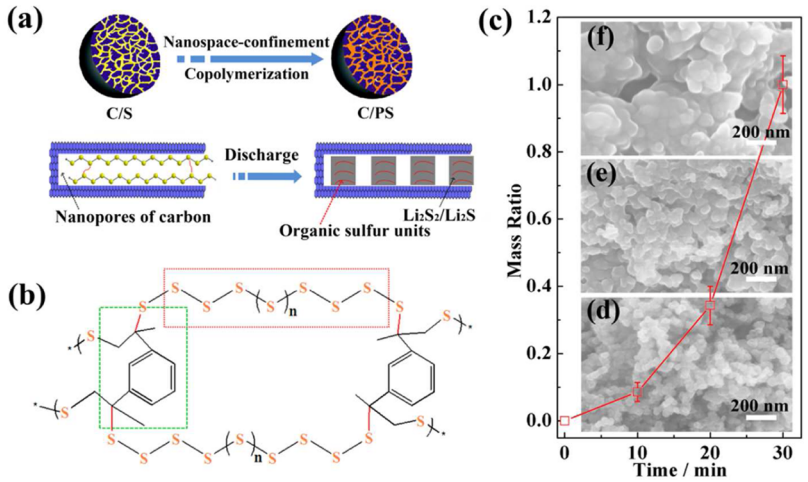

Figure 1. (a) Schematic illustration of preparation procedure of C/PS composites and electrochemical reaction of polymeric sulfur in confined nanopores. (b) Branched and linear units in polymeric sulfur. (c) Mass ratio of DIB to elemental sulfur depends on reaction time. SEM images of C/PS composites prepared at different polymerization times: (d) 10, (e) 20, and (f) 30 min.

on the electrode, tremendously improving the cycling stability. From the viewpoint of preparation, it is necessary to develop another complementary strategy, not only focusing on trapping polysulfides but also controlling the Li_2S_2/Li_2S deposition. A complete solution is to chemically bind sulfur species onto a polymer backbone or carbon surface, such as polyaniline,[17,36] polyacrylonitrile,[37,38] polyvinylidene chloride,[39] and sulfurized carbon.[40] A recent work by Pyun et al. described that polymeric sulfur prepared via inverse vulcanization could suppress irreversible deposition of discharge products.[41,42] The tunable thermomechanical properties of this polymeric sulfur enable fabrication of the well-defined sulfur-rich micropatterned film, which exhibited high specific capacity (823 mAh g^{-1} at 100 cycles) and enhanced capacity retention. However, similar to elemental sulfur, bulk polymeric sulfur still suffered from electronic/ionic insulation and polysulfides intermediates dissolution.[42,43] Inspired by the encapsulation strategy for elemental sulfur, confining polymeric sulfur into conductive matrix may be a promising approach to address these issues. However, encapsulating polymeric sulfur in a confined-space is still challenge because of the different densities of carbon and elemental sulfur. Therefore, it is necessary to develop another complementary strategy to construct porous carbon/polymeric sulfur composites.

Herein, we describe a nanospace-confinement copolymerization strategy for encapsulating polymeric sulfur into porous carbon matrix. The influences of copolymerization time on the components, morphologies, and electrochemical performances of the carbon/polymeric sulfur (C/PS) composites were systemically investigated. The C/PS composite with appropriate sulfur content exhibits enhanced cycling performance with high specific capacity and good rate performances.

RESULTS AND DISCUSSION

The nanospace-confinement copolymerization strategy is schematically presented in Figure 1a. The copolymerization reaction is carried out in seal Teflon autoclave at 190 °C. At this temperature, liquid sulfur is confined in the nanopores of carbon host, keeping an intimate contact with conductive framework. The 1,3-diisopropenylbenzene (DIB) vapor diffuses into pores and reaches the liquid sulfur surface. The cyclo-S_8 is then transferred to polymeric sulfur, keeping contact with the carbon framework. During discharge process, polymeric sulfur goes through a series of polysulfides and generates solid Li_2S_2/Li_2S and organic sulfur units. These organic sulfur units disperse in the solid Li_2S_2/Li_2S phase, which could suppress irreversible deposition. Two critical points with regard to the nanospace-confinement copolymerization should be noted. First, we find that the temperature plays a significant role on the copolymerization kinetic. At low reaction temperature (<180 °C), the low pressure of the DIB vapor restricts the reaction rate. However, a relative high temperature (>200 °C) will severely accelerate the copolymerization reaction and it will be difficult to control the reaction progress. Therefore, a mediated reaction temperature was chosen at 190 °C. Second, as shown in Figure 1b, the polymeric sulfur consists of branched and linear sulfur units. The mass ratio of DIB to sulfur in the C/PS composite reflects the components the branched and linear sulfur units in the polymeric sulfur. The mass ratio could be easily tailored by controlling the copolymerization time (Figure 1c). After reaction for 10 and 20 min, the ratio is about 0.1 and 0.3, respectively. But after 30 min, the ratio dramatically increases to ∼1.0. High ratio corresponds to the low sulfur content in the C/PS composite. To evaluate the contents of sulfur in C/PS composites prepared at different reaction time, TG was conducted. All C/PS composites show large weight loses in the temperature region of 250−350 °C (Supporting Information Figure S1) because of the decomposition of polymeric sulfur. Different from the total sublimation of elemental sulfur, there are still some residual for the polymeric sulfur after thermal treatment. The polymeric sulfur should be transferred to amorphous carbon.

The morphology and nanostructure of the C/PS composites were first characterized through scanning electron microscope (SEM). Pristine C/S composite shows uniform morphology of nanoparticles (Supporting Information Figure S2). Large sulfur particles or aggregations are not observed, indicating that elemental sulfur was fully confined in the nanopores. N_2 adsorption/desorption results (Supporting Information Figure S3) reveal that the porous carbon exhibits high Brunauer−Emmett−Teller (BET) specific surface area (1260 m^2 g^{-1}) and pore volume (1.54 cm^3 g^{-1}). After sulfur encapsulation, the specific surface area and pore volume decrease to 28 m^2 g^{-1} and

DOI: 10.1021/acsami.5b00870
ACS Appl. Mater. Interfaces 2015, 7, 11165−11171

0.08 cm^3 g^{-1} respectively, further demonstrating sulfur occupying the nanopores. Figure 1e−g and Supporting Information Figure S4 display the typical SEM images of C/PS composites prepared at different reaction times. The C/PS composite prepared at 10 min shows similar morphology and sizes distribution with that of C/S composite. The size of the carbon nanoparticles is about 40−60 nm and still remain abundant interparticle pores. In the SEM image, large sulfur or polymer particles or aggregations were not observed, indicating that the polymeric sulfur was completely confined in the pores of carbon. After reaction for 20 min, we find that the size of carbon nanoparticles slightly increases. During the nanospace-confinement copolymerization, the pores are filled with polymeric sulfur and then the polymeric sulfur grows on the surface of carbon nanoparticles. But the interparticle pores could still be observed form the SEM images. After copolymerization for 30 min, the polymeric sulfur grow thicker and carbon nanoparticles were embedded in the polymeric sulfur. Therefore, appropriate reaction time (20 min) is critical for the morphology and nanostructure of C/PS composite. We choose C/PS composite prepared at 20 min for further characterization.

As shown in transmission electron microscopy (TEM) images (Figure 2a, b), the carbon nanoparticles show dense

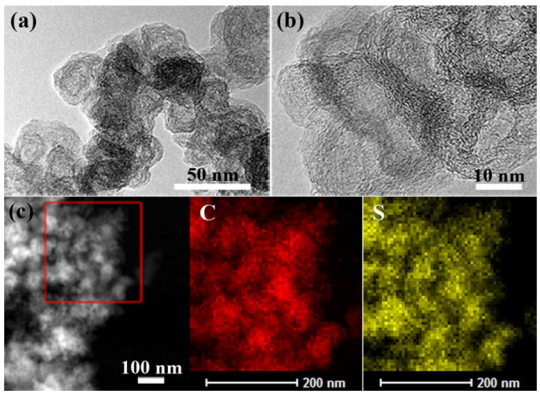

Figure 2. TEM images of (a, b) C/PS composite (20 min), (c) STEM image, and corresponding elemental mapping images of C/PS composite.

pores and graphitized structure, consisting of a few layers of graphene. In addition, no polymeric sulfur layer was observed on the carbon surface, suggesting that polymeric sulfur was confined in the nanopores. The scanning transmission electron microscopy (STEM) image and corresponding element mapping images (Figure 2c) further revels that the uniform dispersion of polymeric sulfur in the porous carbon matrix.

Figure 3a shows the Raman spectra of C/S and C/PS composites. The C/S and C/PS composites show similar Raman spectra and I_D/I_G values (1.27 and 1.25, respectively). The absence of peak of sulfur indicates that sulfur and polymeric sulfur are confined in the pores and shows amorphous structure,[44] which is ascent with the SEM and TEM images. As shown in Figure 3b and Supporting Information Figure S5, the C/S and C/PS composites display similar C 1s and S 2p XPS spectra. The two sulfur spectra both show double peaks, revealing that the sulfur is in the dominated form of elemental sulfur consisting of the S 2p3/2 and S 2p1/2 components.[45,46] But for the C/PS composite, the S 2p peaks shifts to lower binding energy (0.26 eV), corresponding to

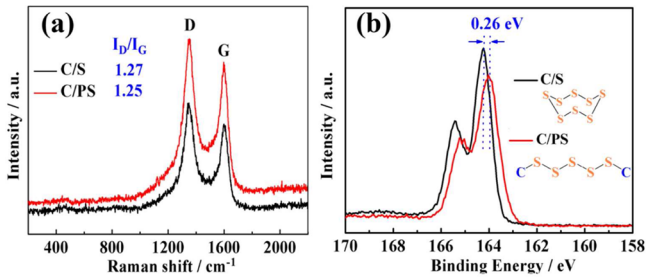

Figure 3. (a) Raman spectra and (b) high-resolution S 2p XPS spectra of C/S and C/PS composite.

weaker S−S bond in polymeric sulfur chain than S−S bond in cyclic sulfur. The weaker binding energy of S−S chain may benefit the kinetics of C/PS electrode. As shown in the S K-edge X-ray absorption near-edge structure (XANES) spectra of polymeric sulfur (Supporting Information Figure S6), the peak at about 2480 eV shift to lower energy. The structure of polymeric sulfur was further characterized via ^{1}H NMR spectrum. The ^{1}H NMR spectrum of polymeric sulfur (Supporting Information Figure S7) confirms the presence of aromatic peaks at δ = 6.5−8.0 ppm, methylene at δ = 2.5−4.0 ppm and methyl protons at δ = 0.7−2.2 ppm.[41] These characteristic peaks confirm the copolymerization of sulfur and DIB.

C/PS and C/S composites were electrochemically test to evaluate the effects of the polymeric sulfur on the electrochemical performances. As shown in of Supporting Information Figure S8a, there are two cathodic peaks and one anodic peak in the CV curves C/PS electrode, which are similar to sulfur cathode.[15,47] The first cathodic at about 2.25 V (vs Li/Li^+) is contributed to the linear sulfur units to long chain polysulfides Li_2S_n ($4 \leq n \leq 8$). The sequential cathodic peak at 2.0 V corresponds to the further reduction of long-chain to Li_2S_2/Li_2S and small organic sulfur units. The anodic peak at ~2.4 V corresponds to the oxidation of Li_2S_2/Li_2S and organic sulfur units.[42] The charge/discharge voltage profiles of C/PS electrode (Supporting Information Figure S8b) shows large overpotential in the first cycle. This suggests that the C/PS electrode requires an activation step, as the interparticle pores of the C/PS composite decrease and it takes some time for the electrolyte to diffuse into the internal surfaces of the active materials.[15]

As shown in Figure 4a, the C/PS electrode shows higher specific capacity and much better cycling performances than that of C/S electrode. The initial specific capacity of C/PS electrode is about 1105 mAh g^{-1} (Specific capacity values were calculated based on the mass of sulfur in the composite.). Moreover, the capacity shows a gradual increase during the first five cycles. After 100 cycles, the capacity of C/PS electrode still remains 889 mAh g^{-1} and capacity retention is up to 80.5%. For C/S electrode, the specific capacity rapidly decreases from 997 to 507 mAh g^{-1}. Even at a high rate of 1 C, the C/PS electrode also exhibits superior cycling performance with high Coulombic efficiency (Figure 4b). After 100 cycles, the capacity is up to 703 mAh g^{-1}. Figure 4c shows the rate performances of C/PS electrode. At rates of 0.2, 0.5, 1, 2, and 5 C, the capacities are 1094, 905, 815, 751, and 681 mAh g^{-1}. The charge/discharge voltage profile of C/PS still remains the charge/discharge plateau (Figure 4d) at high current rates, which further indicates the excellent rate performance. The enhanced performance of C/SP composite electrode is associated with

DOI: 10.1021/acsami.5b00870
ACS Appl. Mater. Interfaces 2015, 7, 11165−11171

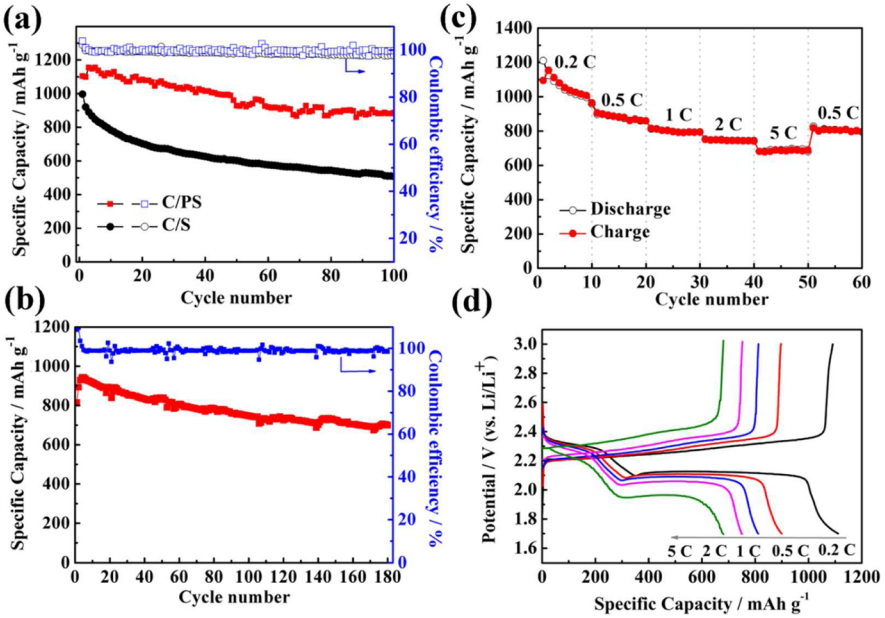

Figure 4. Electrochemical performances of C/PS (20 min) electrode: (a) cycling performances of C/S and C/PS electrodes at a current rate of 0.5 C, (b) cycling performance of C/PS electrode at 1 C, (c) rate performance of C/PS electrode, and (d) charge/discharge voltage profile of C/PS electrode at different rates.

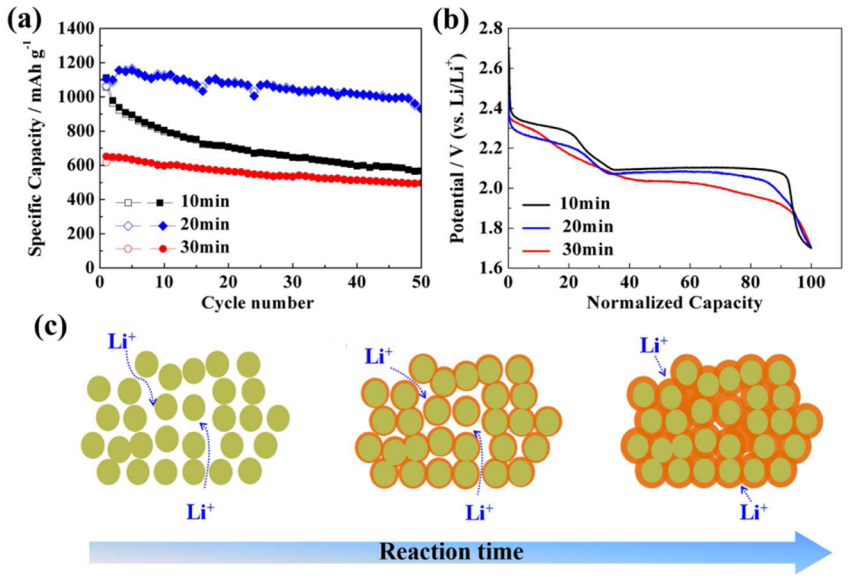

Figure 5. (a) Comparison of cycling performances of different C/PS composites at 0.5 C. (b) Normalized discharge curves of C/PS composites at 0.5 C. (c) Schematic illustration of lithium ion diffusion in C/PS composites with different morphologies.

the nanostructure with polymeric sulfur confined in the nanospace. The carbon matrix with high electric conductivity and high specific surface area is favorable for the electronic/ionic transport and suppress the dissolution of polysulfides in the electrolyte. Compared with the C/S composite, the organic sulfur in the discharge product could prevent the irreversible deposition of Li_2S_2/Li_2S on the surface of electrode, which also enhances the electronic/ionic transport.

To investigate the effects of the ratio on the electrochemical performance, we compared the electrochemical performances of C/PS composites prepared at different reaction time. Figure 5a shows the cycling performances of three C/PS composites at a current density of 0.5 C. For C/PS composite with low ratio (10 min), the electrode shows a high specific capacity but poor cycling stability. The initial capacity is about 1112 mAh g^{-1}. After 50 cycles, the capacity is only about 566 mAh g^{-1}. The capacity retention is only about 51%. As discussed above, when the copolymerization increases to 20 min, the C/PS exhibits best electrochemical performance with high specific capacity and cycling stability. However, when the copolymerization time increases to 30 min, the C/PS composite electrode shows good cycling performance but low capacity. Figure 5b shows the typical normalized discharge curves of C/PS composite electrodes. For C/PS composites prepared under 10 and 20 min, the discharge curves show two obvious discharge plateaus. However, C/PS composite prepared under long reaction time (30 min), the curve shows large overpotential, which may be the main reason for low capacity. We propose that the reaction

DOI: 10.1021/acsami.5b00870
ACS Appl. Mater. Interfaces 2015, 7, 11165−11171

time-dependent differences can be partially traced to the sulfur contents and morphologies. As schematically presented in Figure 5c, with short reaction time (10 and 20 min), the C/PS composite still remain porous nanostructure with interparticle pores (Figure 2a–d), which favors the diffusion of lithium ion during charge/discharge process. However, when the copolymerization time increases to 30 min, polymeric sulfur occupied the interparticle pores and the carbon nanoparticles was completely embedded in the insulating polymeric sulfur. The polymeric sulfur shell block the electron and lithium ion pathway, thus leading to low electrochemical utilization of active material.

To deeply investigate the effects of organic sulfur on the deposition of Li_2S_2/Li_2S on the surface of electrodes, morphology characterizations and EIS of the electrodes after cycling (at fully charge state) were conducted. As presented in Figure 6a, dense discharge product aggregations could be obviously observed on the surface of C/S electrode. These detrimental products format from the deep discharge of sulfur and the strong reduction of soluble polysulfides in the electrolyte. These inactive products "paste" on the C/S electrode not only lead to loss of active materials, but also block the electric/ionic transport, both of which could result in capacity fading. In contrast, the morphology of C/PS (20 min) electrode before (Supporting Information Figure S9) and after cycling (Figure 6b) show no significant change. The similar morphologies of C/PS before and after cycling indicate the uniform deposition of Li_2S_2/Li_2S. The EIS spectra of C/S and C/PS electrodes (Supporting Information Figure S10) after cycling were composed of a semicircle in the high-frequency domain and a straight line in the low-frequency region. The semicircle in the high-frequency domain corresponds to the charge-transfer process, and the straight line in the low-frequency domain corresponds to a semi-infinite Warburg diffusion process.[19] Obviously, the C/PS electrode shows lower charge-transfer resistance and Warburg diffusion resistance, indicating faster electronic/ionic transport in the C/PS electrode. The reason may be attributed to the presence of the organic sulfur units.[42] The organic sulfur units disperse in insoluble/insulating discharge product phase and suppress the irreversible deposition of insoluble products. Therefore, the polymeric sulfur confined in the nanopores could significantly suppress the aggregation of insulated Li_2S_2/Li_2S on the electrode surface during cycling.

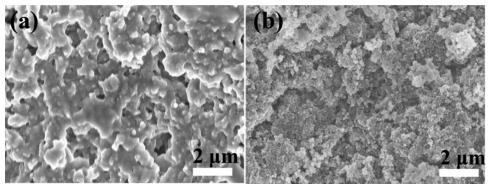

Figure 6. SEM images of (a) C/S and (b) C/PS electrodes after cycling.

CONCLUSION

In summary, we describe a nanospace-confinement copolymerization strategy for preparation of C/PS composites with polymeric sulfur encapsulated in the nanopores of carbon. Such nanostructure favor rapid electronic/ionic transport and alleviate the solubility of polysulfides during the charge/discharge process. The organic sulfur units disperse in insoluble/insulating discharge product phase and suppress the irreversible deposition of insoluble discharge products. These combined unique features permit the C/PS electrode to exhibit excellent cycling stability with high rate capability. At a current rate of 0.5 C, the C/PS electrode exhibits a high specific capacity of 1105 mAh g^{-1} and a capacity retention of 81% after 100 cycles. The strategy described here may provide new avenues for the future development of polymeric sulfur-based Li–S batteries with high specific capacity and excellent cycling performance.

EXPERIMENTAL SECTION

Preparation of C/S and C/PS Composites. The C/S composite with a sulfur content of 70 wt % was prepared through a melt–diffusion method as described in previous reports.[11,17] Typically, 150 mg of commercial conductive carbon black (Ketjenblack EC600JD) and 350 mg of sublimed sulfur (chemical grade) were ground together and heated to 155 °C for 12 h. The C/PS composites were prepared through a nanospace-confinement copolymerization strategy. Typically, 100 mg of C/S composite was added to a 25 mL beaker and then placed in a 100 mL autoclave. Then 1 mL of 1,3-diisopropenylbenzene (DIB) was dropped into the autoclave and heated at 190 °C for different times. C/PS composites were carefully collected and the mass ratio of DIB to sulfur was calculated after reaction for different times. For comparison, C/S composite was also treated under same conditions but without DIB.

Characterization. The morphologies of as-prepared C/S and C/PS composites were examined by scanning electron microscope (Hitachi 4800), transmission electron microscopy (JEOL JEM-2010) and scanning transmission electron microscopy (Tecnai G2 F20). Raman spectra were conducted on the HORIBA Scientific LabRAM HR Raman spectrometer system with a 532.4 nm laser. The X-ray photoelectron spectroscopy analysis was performed on a PerkinElmer PHI 550 spectrometer with Al Kα (1486.6 eV) as the X-ray source. Thermogravimetric analysis was conducted on a TG-DSC instrument (NETZSCH STA 409 PC) under nitrogen protection at a heating rate of 10 °C min^{-1} from 30 to 600 °C. The N_2 adsorption–desorption isotherms of the samples were conducted by a Micromeritics BK122T-B analyzer. The specific surface area was calculated using the Brunauer–Emmett–Teller method. The total pore volume and pore size distribution were obtained from Barret–Joyner–Halenda adsorption cumulative volume of pores. The XANES experiment is performed at 4B7A beamline, Beijing Synchrotron Radiation Facility (BSRF), using a Si (111) crystal monochromator. The XANES spectra were collected in a total electron yield (TEY) mode. The 1H-NMR were performed with a Bruker DRX-400 NMR spectrometer at room temperature using D-chloroform ($CDCl_3$) as solvent. The C/PS composite was dispersed in $CHCl_3$ to dissolve polymeric sulfur. To obtain the polymeric sulfur, then the supernatants was collected and dried under vacuum at 60 °C.

Electrochemical Measurements. Electrochemical characterization was carried out by galvanostatic cycling in a CR2016-type coin cell. The working electrodes were prepared at a slurry coating procedure. The slurry consisted of active material (C/S or C/PS composites), acetylene black, and polyvinylidene fluoride at a weight ratio of 70:20:10 in *N*-methylpyrrolidinone and was uniformly spread on an aluminum foil current collector and then was dried at 65 °C for 12 h. Test cells were assembled in an argon-filled glovebox. Lithium foil was used as the counter electrode and the separator was Celgard 2400. The electrolyte was composed of 1 M bis(trifluoromethane) sulfonimide lithium (LiTFSI) salt and 0.1 M $LiNO_3$ additive dissolved in a mixed solvent of 1,3-dioxolane (DOL) and 1,2-dimethoxyethane (DME) (1:1 by volume). Cyclic voltammetry (CV) and electrochemical impedance spectra (EIS) were performed on a Zive SP2 electrochemical workstation (WonATech Co. Ltd., Korea). EIS was conducted at in the frequency range of 10^5–10^{-2} Hz with the amplitude of 5 mV. Galvanostatical charge/discharge cycle was

DOI: 10.1021/acsami.5b00870
ACS Appl. Mater. Interfaces 2015, 7, 11165–11171

performed on a CT2001A cell test instrument (LAND Electronic Co.) in the potential window of 1.7−3.0 V.

■ ASSOCIATED CONTENT

Supporting Information

TG curves of C/S and C/PS composites, SEM images of C/S composite, N_2 adsorption/desorption isotherms and pore size distribution of carbon and C/S composite, SEM images of C/PS composites prepared at different polymerization times, high-resolution C 1s XPS spectra of C/S and C/PS composites, CV curves and galvanostatic charge/discharge profiles of C/SP composite electrode, SEM images of C/PS composite electrode before cycling. The Supporting Information is available free of charge on the ACS Publications website at DOI: 10.1021/acsami.5b00870.

■ AUTHOR INFORMATION

Corresponding Author

*E-mail: azhangxg@163.com.

Notes

The authors declare no competing financial interest.

■ ACKNOWLEDGMENTS

The work was funded by the National Key Basic Research Program 973 (No. 2014CB239701), Natural Science Foundation of Jiangsu Province (No. BK2011030, No. BK2011740), NSFC (No. 21173120, No. 51372116), Fundamental Research Funds for the Central Universities of NUAA (NP2014403), and the Priority Academic Program Development of Jiangsu Higher Education Institutions (PAPD). B.D. and J.P. are grateful to Funding of Jiangsu Innovation Program for Graduate Education (CXZZ13_0158), Outstanding Doctoral Dissertation in NUAA (BCXJ13-13), and the Fundation of Graduate Innovation Center in NUAA (kfjj130219). The authors thank beamline 4B7A (BSRF) for providing the beam time.

■ REFERENCES

(1) Bruce, P. G.; Freunberger, S. A.; Hardwick, L. J.; Tarascon, J. M. Li−O_2 and Li−S Batteries with High Energy Storage. *Nat. Mater.* **2012**, *11*, 19−29.

(2) Manthiram, A.; Fu, Y. Z.; Su, Y. S. Challeges and Prospects of Lithium−Sulfur. *Acc. Chem. Res.* **2013**, *46*, 1125−1134.

(3) Zhang, C. F.; Wu, H. B.; Yuan, C. Z.; Guo, Z. P.; Lou, X. W. Confining Sulfur in Double-Shelled Hollow Carbon Spheres for Lithium−Sulfur Batteries. *Angew. Chem., Int. Ed.* **2012**, *51*, 9592−9595.

(4) Yin, Y.-X.; Xin, S.; Guo, Y.-G.; Wan, L.-J. Lithium−Sulfur Batteries: Electrochemistry, Materials, and Prospects. *Angew. Chem., Int. Ed.* **2013**, *52*, 13186−13200.

(5) Li, L.; Ruan, G.; Peng, Z.; Yang, Y.; Fei, H.; Raji, A. R. O.; Samuel, E. L. G.; Tour, J. M. Enhanced Cycling Stability of Lithium Sulfur Batteries Using Sulfur Polyaniline−Graphene Nanoribbon Composite Cathodes. *ACS Appl. Mater. Interfaces* **2014**, *6*, 15033−15039.

(6) Ding, B.; Yuan, C. Z.; Shen, L. F.; Xu, G. Y.; Nie, P.; Lai, Q. X.; Zhang, X. G. Chemically Tailoring the Nanostructure of Graphene Nanosheets to Confine Sulfur for High-Performance Lithium−Sulfur Batteries. *J. Mater. Chem. A* **2012**, *1*, 1096−1101.

(7) Wu, H. L.; Huff, L. A.; Gewirth, A. A. In Situ Raman Spectroscopy of Sulfur Speciation in Lithium−Sulfur Batteries. *ACS Appl. Mater. Interfaces* **2015**, *7*, 1709−1719.

(8) Agostini, M.; Hassoun, J.; Liu, J.; Jeong, M.; Nara, H.; Momma, T.; Osaka, T.; Sun, Y. K.; Scrosati, B. A Lithium-Ion Sulfur Battery Based on a Carbon-Coated Lithium−Sulfide Cathode and an Electrodeposited Silicon-Based Anode. *ACS Appl. Mater. Interfaces* **2014**, *6*, 10924−10928.

(9) Sun, F. G.; Wang, J. T.; Chen, H. C.; Li, W. C.; Qiao, W. M.; Long, D. H.; Ling, L. C. High Efficiency Immobilization of Sulfur on Nitrogen-Enriched Mesoporous Carbons for Li−S Batteries. *ACS Appl. Mater. Interfaces* **2013**, *5*, 5630−5638.

(10) Seh, Z. W.; Li, W. Y.; Cha, J. J.; Zheng, G. Y.; Yang, Y.; McDowell, M. T.; Hsu, P. C.; Cui, Y. Sulphur−TiO_2 Yolk-Shell Nanoarchitecture with Internal Void Space for Long-Cycle Lithium−Sulphur Batteries. *Nat. Commun.* **2013**, *4*, 1331.

(11) Zhou, W. D.; Yu, Y. C.; Chen, H.; DiSalvo, F. J.; Abruna, H. D. Yolk−Shell Structure of Polyaniline-Coated Sulfur for Lithium−Sulfur Batteries. *J. Am. Chem. Soc.* **2013**, *135*, 16736−16743.

(12) Hassoun, J.; Scrosati, B. Moving to a Solid-State Configuration: A Valid Approach to Making Lithium-Sulfur Batteries Viable for Practical Applications. *Adv. Mater.* **2010**, *22*, 5198−5201.

(13) Ji, X. L.; Lee, K. T.; Nazar, L. F. A Highly Ordered Nanostructured Carbon−Sulphur Cathode for Lithium−Sulphur Batteries. *Nat. Mater.* **2009**, *8*, 500−506.

(14) Liang, C. D.; Dudney, N. J.; Howe, J. Y. Hierarchically Structured Sulfur/Carbon Nanocomposite Material for High-Energy Lithium Battery. *Chem. Mater.* **2009**, *21*, 4724−4730.

(15) Elazari, R.; Salitra, G.; Garsuch, A.; Panchenko, A.; Aurbach, D. Sulfur-Impregnated Activated Carbon Fiber Cloth as a Binder-Free Cathode for Rechargeable Li−S Batteries. *Adv. Mater.* **2011**, *23*, 5641−5644.

(16) Jayaprakash, N.; Shen, J.; Moganty, S. S.; Corona, A.; Archer, L. A. Porous Hollow Carbon@Sulfur Composites for High-Power Lithium−Sulfur Batteries. *Angew. Chem., Int. Ed.* **2011**, *50*, 5904−5908.

(17) Xiao, L.; Cao, Y.; Xiao, J.; Schwenzer, B.; Engelhard, M. H.; Saraf, L. V.; Nie, Z.; Exarhos, G. J.; Liu, J. A Soft Approach to Encapsulate Sulfur: Polyaniline Nanotubes for Lithium−Sulfur Batteries with Long Cycle Life. *Adv. Mater.* **2012**, *24*, 1176−1181.

(18) Chen, H. W.; Dong, W. L.; Ge, J.; Wang, C. H.; Wu, X. D.; Lu, W.; Chen, L. W. Ultrafine Sulfur Nanoparticles in Conducting Polymer Shell as Cathode Materials for High Performance Lithium/Sulfur Batteries. *Sci. Rep.* **2013**, *3*, 1910.

(19) Li, G. C.; Li, G. R.; Ye, S. H.; Gao, X. P. A Polyaniline-Coated Sulfur/Carbon Composite with an Enhanced High-Rate Capability as a Cathode Material for Lithium/Sulfur Batteries. *Adv. Energy Mater.* **2012**, *2*, 1238−1245.

(20) Wu, F.; Chen, J. Z.; Chen, R. J.; Wu, S. X.; Li, L.; Chen, S.; Zhao, T. Sulfur/Polythiophene with a Core/Shell Structure: Synthesis and Electrochemical Properties of the Cathode for Rechargeable Lithium Batteries. *J. Phys. Chem. C* **2011**, *115*, 6057−6063.

(21) Xin, S.; Gu, L.; Zhao, N. H.; Yin, Y. X.; Zhou, L. J.; Guo, Y. G.; Wan, L. J. Smaller Sulfur Molecules Promise Better Lithium−Sulfur Batteries. *J. Am. Chem. Soc.* **2012**, *134*, 18510−18513.

(22) Lee, J. T.; Zhao, Y.; Thieme, S.; Kim, H.; Oschatz, M.; Borchardt, L.; Magasinski, A.; Cho, W.-I.; Kaskel, S.; Yushin, G. Sulfur-Infiltrated Micro- and Mesoporous Silicon Carbide-Derived Carbon Cathode for High-Performance Lithium Sulfur Batteries. *Adv. Mater.* **2013**, *25*, 4573−4579.

(23) Tang, C.; Zhang, Q.; Zhao, M.-Q.; Huang, J.-Q.; Cheng, X.-B.; Tian, G.-L.; Peng, H.-J.; Wei, F. Nitrogen-Doped Aligned Carbon Nanotube/Graphene Sandwiches: Facile Catalytic Growth on Bifunctional Natural Catalysts and Their Applications as Scaffolds for High-Rate Lithium−Sulfur Batteries. *Adv. Mater.* **2014**, *26*, 6100−6105.

(24) Zhao, Y.; Wu, W. L.; Li, J. X.; Xu, Z. C.; Guan, L. H. Encapsulating MWNTs into Hollow Porous Carbon Nanotubes: A Tube-in-Tube Carbon Nanostructure for High-Performance Lithium−Sulfur Batteries. *Adv. Mater.* **2014**, *26*, 5113−5118.

(25) Li, Z.; Jiang, Y.; Yuan, L.; Yi, Z.; Wu, C.; Liu, Y.; Strasser, P.; Huang, Y. A Highly Ordered Meso@Microporous Carbon-Supported Sulfur@Smaller Sulfur Core−Shell Structured Cathode for Li−S Batteries. *ACS Nano* **2014**, *8*, 9295−9303.

(26) Ji, L.; Rao, M.; Zheng, H.; Zhang, L.; Li, Y.; Duan, W.; Guo, J.; Cairns, E. J.; Zhang, Y. Graphene Oxide as a Sulfur Immobilizer in

High Performance Lithium/Sulfur Cells. *J. Am. Chem. Soc.* **2011**, *133*, 18522−18525.
(27) Song, J.; Xu, T.; Gordin, M. L.; Zhu, P.; Lv, D.; Jiang, Y.-B.; Chen, Y.; Duan, Y.; Wang, D. Nitrogen-Doped Mesoporous Carbon Promoted Chemical Adsorption of Sulfur and Fabrication of High-Areal-Capacity Sulfur Cathode with Exceptional Cycling Stability for Lithium−Sulfur Batteries. *Adv. Funct. Mater.* **2014**, *24*, 1243−1250.
(28) Qiu, Y.; Li, W.; Zhao, W.; Li, G.; Hou, Y.; Liu, M.; Zhou, L.; Ye, F.; Li, H.; Wei, Z.; Yang, S.; Duan, W.; Ye, Y.; Guo, J.; Zhang, Y. High-Rate, Ultra-Long-Cycle-Life Lithium/Sulfur Batteries Enabled by Nitrogen-Doped Graphene. *Nano Lett.* **2014**, *14*, 4821−4827.
(29) Guo, J. C.; Yang, Z. C.; Yu, Y. C.; Abruna, H. D.; Archer, L. A. Lithium−Sulfur Battery Cathode Enabled by Lithium−Nitrile Interaction. *J. Am. Chem. Soc.* **2013**, *135*, 763−767.
(30) Zheng, S.; Yi, F.; Li, Z.; Zhu, Y.; Xu, Y.; Luo, C.; Yang, J.; Wang, C. Copper-Stabilized Sulfur−Microporous Carbon Cathodes for Li−S Batteries. *Adv. Funct. Mater.* **2014**, *24*, 4156−4163.
(31) Kim, H.; Lee, J. T.; Lee, D.-C.; Magasinski, A.; Cho, W.-i.; Yushin, G. Plasma-Enhanced Atomic Layer Deposition of Ultrathin Oxide Coatings for Stabilized Lithium−Sulfur Batteries. *Adv. Energy Mater.* **2013**, *3*, 1308−1315.
(32) Hassoun, J.; Scrosati, B. A High-Performance Polymer Tin Sulfur Lithium Ion Battery. *Angew. Chem., Int. Ed.* **2010**, *49*, 2371−2374.
(33) Xu, R.; Belharouak, I.; Zhang, X. F.; Chamoun, R.; Yu, C.; Ren, Y.; Nie, A.; Shahbazian-Yassar, R.; Lu, J.; Li, J. C. M.; Amine, K. Insight into Sulfur Reactions in Li−S Batteries. *ACS Appl. Mater. Interfaces* **2014**, *6*, 21938−21945.
(34) Su, Y.-S.; Fu, Y.; Cochell, T.; Manthiram, A. A Strategic Approach to Recharging Lithium−Sulphur Batteries for Long Cycle Life. *Nat. Commun.* **2013**, *4*, 2985.
(35) Zheng, J.; Gu, M.; Wang, C.; Zuo, P.; Koech, P. K.; Zhang, J.-G.; Liu, J.; Xiao, J. Controlled Nucleation and Growth Process of Li_2S_2/Li_2S in Lithium−Sulfur Batteries. *J. Electrochem. Soc.* **2013**, *160*, A1992−A1996.
(36) Wen, T. C.; Huang, L. M.; Gopalan, A. Electrochemical Synthesis of a Polyaniline-Based Conducting Copolymer with −S−S− Links. *J. Electrochem. Soc.* **2001**, *148*, D9−D17.
(37) Wang, J. L.; Yang, J.; Xie, J. Y.; Xu, N. X. A Novel Conductive Polymer−Sulfur Composite Cathode Material for Rechargeable Lithium Batteries. *Adv. Mater.* **2002**, *14*, 963−965.
(38) Yin, L.; Wang, J.; Yang, J.; Nuli, Y. A Novel Pyrolyzed Polyacrylonitrile−Sulfur@MWCNT Composite Cathode Material for High-Rate Rechargeable Lithium/Sulfur Batteries. *J. Mater. Chem.* **2011**, *21*, 6807−6810.
(39) Duan, B.; Wang, W.; Wang, A.; Yuan, K.; Yu, Z.; Zhao, H.; Qiu, J.; Yang, Y. Carbyne Polysulfide as a Novel Cathode Material for Lithium/Sulfur Batteries. *J. Mater. Chem. A* **2013**, *1*, 13261−13267.
(40) Zhang, S. S. Sulfurized Carbon: A Class of Cathode Materials for High Performance Lithium/Sulfur Batteries. *Front. Energy Res.* **2013**, *1*, 10.
(41) Chung, W. J.; Griebel, J. J.; Kim, E. T.; Yoon, H.; Simmonds, A. G.; Ji, H. J.; Dirlam, P. T.; Glass, R. S.; Wie, J. J.; Nguyen, N. A.; Guralnick, B. W.; Park, J.; Somogyi, A.; Theato, P.; Mackay, M. E.; Sung, Y.-E.; Char, K.; Pyun, J. The Use of Elemental Sulfur as an Alternative Feedstock for Polymeric Materials. *Nat. Chem.* **2013**, *5*, 518−524.
(42) Simmonds, A. G.; Griebel, J. J.; Park, J.; Kim, K. R.; Chung, W. J.; Oleshko, V. P.; Kim, J.; Kim, E. T.; Glass, R. S.; Soles, C. L.; Sung, Y.-E.; Char, K.; Pyun, J. Inverse Vulcanization of Elemental Sulfur to Prepare Polymeric Electrode Materials for Li−S Batteries. *ACS Macro Lett.* **2014**, *3*, 229−232.
(43) Sun, Z.; Xiao, M.; Wang, S.; Han, D.; Song, S.; Chen, G.; Meng, Y. Sulfur-Rich Polymeric Materials with Semi-Interpenetrating Network Structure as a Novel Lithium−Sulfur Cathode. *J. Mater. Chem. A* **2014**, *2*, 9280−9286.
(44) Wang, B.; Li, K. F.; Su, D. W.; Ahn, H. J.; Wang, G. X. Superior Electrochemical Performance of Sulfur/Graphene Nanocomposite Material for High-Capacity Lithium−Sulfur Batteries. *Chem.—Asian J.* **2012**, *7*, 1637−1643.
(45) Zhou, G.; Yin, L. C.; Wang, D. W.; Li, L.; Pei, S.; Gentle, I. R.; Li, F.; Cheng, H.-M. Fibrous Hybrid of Graphene and Sulfur Nanocrystals for High-Performance Lithium−Sulfur Batteries. *ACS Nano* **2013**, *7*, 5367−5375.
(46) Zhang, L.; Ji, L. W.; Glans, P. A.; Zhang, Y. G.; Zhu, J. F.; Guo, J. H. Electronic Structure and Chemical Bonding of a Graphene Oxide-Sulfur Nanocomposite for Use in Superior Performance Lithium−Sulfur Cells. *Phys. Chem. Chem. Phys.* **2012**, *14*, 13670−13675.
(47) Yang, X.; Zhang, L.; Zhang, F.; Huang, Y.; Chen, Y. Sulfur-Infiltrated Graphene-Based Layered Porous Carbon Cathodes for High-Performance Lithium−Sulfur Batteries. *ACS Nano* **2014**, *8*, 5208−5215.

DOI: 10.1021/acsami.5b00870
ACS Appl. Mater. Interfaces 2015, 7, 11165−11171